Brigham Young University
BYU ScholarsArchive

Faculty Publications

1994

The Impact of Coal Pyrolysis on Combustion

Peter R. Solomon
Advanced Fuel Research

Thomas H. Fletcher
Brigham Young University, tom_fletcher@byu.edu

Follow this and additional works at: https://scholarsarchive.byu.edu/facpub

 Part of the Chemical Engineering Commons

Original Publication Citation

Solomon, P. R. and T. H. Fletcher, "The Impact of Pyrolysis in Combustion," an invited review paper, Twenty-Fifth Symposium (International) on Combustion, 463-474 (1994). DOI: 10.1016/S0082-0784(06)80675-2

BYU ScholarsArchive Citation

Solomon, Peter R. and Fletcher, Thomas H., "The Impact of Coal Pyrolysis on Combustion" (1994). *Faculty Publications*. 6157.
https://scholarsarchive.byu.edu/facpub/6157

This Peer-Reviewed Article is brought to you for free and open access by BYU ScholarsArchive. It has been accepted for inclusion in Faculty Publications by an authorized administrator of BYU ScholarsArchive. For more information, please contact ellen_amatangelo@byu.edu.

Twenty-Fifth Symposium (International) on Combustion/The Combustion Institute, 1994/pp. 463–474

INVITED TOPICAL REVIEW

IMPACT OF COAL PYROLYSIS ON COMBUSTION

PETER R. SOLOMON
Advanced Fuel Research, Inc.
87 Church Street, East Hartford, CT 06108, USA

AND

THOMAS H. FLETCHER
Department of Chemical Engineering
Brigham Young University
350 CB, Provo, Utah 84602, USA

The pyrolysis process has impacts throughout coal combustion. The roles of pyrolysis in various aspects of the coal combustion process are described, including the devolatilization yield, nitrogen release, softening and swelling, soot formation, and char reactivity. These processes can be understood and quantitatively predicted using recently developed network pyrolysis models that describe the transformation of the coal's chemical structure. The models are described and examples of their predictive ability for important coal combustion phenomena are presented.

Introduction

It has been said that, other than the volatile yield, the details of coal pyrolysis are unimportant in combustion. The argument is that pyrolysis occurs rapidly, whereas char oxidation occurs slowly, and thus, it is the latter that controls the overall process. But a closer examination suggests that pyrolysis exerts its influence throughout the life of the solid particle from injection to burnout.

When coal enters a hot furnace and is heated, it may soften and swell. These processes are a function of the coal's fluidity, which is mostly determined by pyrolysis. The fluidity of the coal is controlled by the way bond breaking and cross-linking reactions affect the coal's organic matrix. These reactions can be drastically influenced by chemical changes in the coal induced by weathering. The swelling of the coal particle is caused by expanding bubbles of gaseous volatiles produced by pyrolysis in the viscous liquid. Depending on the heating rate, temperature, and particle size, either a particle may swell or the bubbles may rupture. Coal softening affects the porosity and internal surface area of the resulting char. Softening, therefore, affects the ignition, particle trajectory in the furnace, reactivity, and eventual fragmentation.

The ignition of the coal may be due to heterogeneous oxidation of the particle or to homogeneous combustion of the pyrolysis volatiles. The relative rates of solid oxidation and volatile evolution determine which type of ignition occurs first.

The pyrolysis process controls the product distribution of tar, char, and gases. The tar is the primary source of soot, which dominates radiative heat transfer in the volatile flame region. The rates and forms of sulfur and nitrogen evolution are initially controlled by pyrolysis. Char burnout is dependent on the amount of char after devolatilization, particle morphology (after possible melting and swelling) and intrinsic reactivity. The intrinsic reactivity is modified as pyrolysis reactions condense the organic network.

Finally, the chemistry and size distribution of the ash (important to slagging and fouling) are influenced by char temperature and morphology during oxidation. Particle temperature, which impacts the melting, vaporization, and chemical reactions of the minerals, is related to a variety of factors, including char intrinsic reactivity and morphology. Both of these are controlled by pyrolysis. Particle morphology affects the char fragmentation, which influences the size of ash particles.

Any attempt to quantitatively predict how pyrolysis affects these combustion events requires a detailed pyrolysis model; a single global devolatilization rate is not sufficient. The detailed model must describe (1) the thermal decomposition of the coal's organic matrix, (2) the release of network fragments as tar, (3) the release of light gas species from decomposition of functional groups attached to the condensed ring structures, and (4) the condensation or cross-linking of the organic matrix and the accompanying formation of gas species.

Several recent detailed pyrolysis models based on statistical decomposition of networks or chains that represent the coal's organic matrix have been pro-

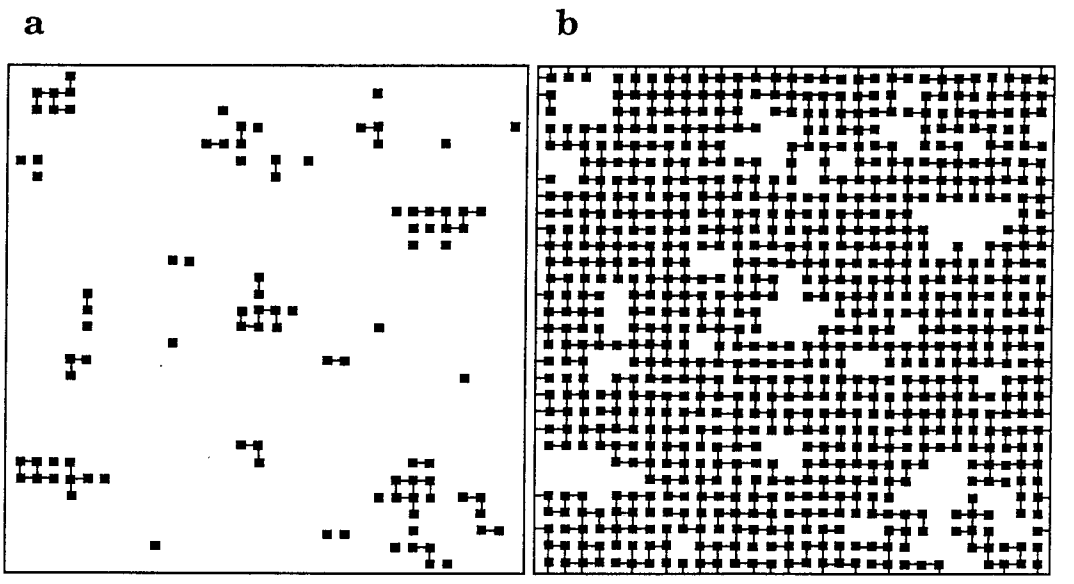

FIG. 1. Monte Carlo simulations of a square lattice with coordination number of 4 and 55% of the bridges intact, showing (a) the 11% of the clusters that are detached from the lattice and (b) the clusters still attached to the matrix [12].

posed to describe these processes [1–21]. This paper presents the general concepts of these models and describes the relationship between pyrolysis events and the predictions of the models. The relationship between pyrolysis and char reactivity is not reviewed in detail due to space limitations.

Network Models of Pyrolysis

Pyrolysis models have progressed from empirical relationships to models that are based on the chemical structure of the parent coal. There have been numerous reviews of the empirical models that employ single reaction rate decomposition, parallel reaction decompositions, and distributed activation energy rate decomposition. In this paper, we consider only the recent detailed chemical models. Additional comparisons of these network models are available [13,22]. Three network models of coal pyrolysis that approximate the breakdown of the macromolecular coal structure are the functional group, depolymerization, vaporization, and cross-linking (FG-DVC) model [10,21]; the FLASHCHAIN model [16–18]; and the chemical percolation devolatilization (CPD) model [12,14,19].

The basic approach of the network pyrolysis models is to treat the coal macromolecular structure as a lattice of aromatic clusters (monomers) connected by aliphatic bridges. The geometry, or degree of branching of the network, is expressed by the number of possible attachments per cluster, often called the coordination number ($\sigma + 1$). A coordination number of 2.0 represents a linear chain polymer, while higher coordination numbers represent more complex cross-linked structures. Network models assign molecular weights to the monomers and use statistics to determine the rate of breaking of interconnecting bridges based on some distribution of activation energies. Oligomers that are disconnected from the coal lattice by bridge breaking become metaplast and tar.

The importance of lattice statistics in the breakup of the coal macromolecule is illustrated in Fig. 1 for a square lattice (coordination number of 4). After 55% of the connecting bridges are broken at random, only 11% of the clusters are detached from the original lattice. The fraction of liberated fragments from a lattice is a nonlinear function of the fraction of ruptured bridges. The molecular weight distribution of the fragments depends on the coordination number. Both Monte Carlo methods and percolation statistics have been used to calculate the relationship between the number of ruptured bridges and the distribution of fragments. Monte Carlo methods give maximum flexibility in specifying the initial lattice structure, but percolation lattice statistics permit a closed-form solution, which reduces computational time. Approaches using percolation statistics assume that coal can be represented as either a linear chain [3–5,16–18] or a loopless tree structure, called a Bethe lattice [6–9,12,13,19,21]. Since the coal macromolecule is large, the Bethe lattice approximation does not introduce significant error [12]. A model using one

bridge network with a coordination number for the initial bridges and a separate interconnected network with a second coordination number for cross-linking, referred to as a 2-σ model, was developed to increase the flexibility and match both initial extract yields and final tar yields [13,21].

As shown in Fig. 1, the lattice statistics determine a distribution of oligomers (monomers, dimers, etc.). The fragment molecular weight is calculated from the oligomer number and the weight of the interconnecting bridges and side attachments. Generalized vapor pressure expressions have been developed for coal tar [23,24] based on molecular weight and temperature. The vapor pressure of the detached material determines the partition between the vapor (tar) and the liquid (metaplast). Tar vapor is convected from the particle along with other light gases, while the metaplast remains in the char until (a) higher temperatures are achieved to vaporize more metaplast or (b) subsequent cross-linking reactions occur to reattach the metaplast to the char. Since the light gases within the particle will be at the ambient pressure and the heavy species will be at their vapor pressure (to first order, independent of the ambient pressure), the molar ratio of tar to light gases will decrease with increasing pressure in agreement with the observed effect of pressure on tar yields.

Recent measurements of the chemical structure of coals and chars by ^{13}C NMR solid-state spectroscopy [25,26] provide input parameters for the network models. These measurements determine the following: the total number of attachments per cluster ($\sigma + 1$), the fraction (p) of attachments that are bridges rather than side chains, the average molecular weight per monomer cluster, and the average molecular weight per side chain. Solvent swelling characteristics and pyridine extract yields have also been used to determine input parameters [10,21].

The three network models use several similar assumptions: (1) a network that decomposes to form fragments when bridges between aromatic clusters are randomly broken, (2) a vapor-liquid equilibrium model to determine the molecular weight and amount of the cluster released as tar, and (3) a cross-linking model that reattaches the clusters. Differences between the models are related to how the network is described. The essential features of the network is the coordination number. A coordination number of 2 is assumed in FLASHCHAIN. The coordination number in FG-DVC is based on the initial extract yield and pyrolysis tar yield. This number is near 2 (i.e., chainlike). However, during pyrolysis, new bridges may form so that the cross-linked char can have a higher coordination number. This variable coordination number was implemented both with a Monte Carlo simulation and with the 2-σ percolation theory. This feature of FG-DVC allows it to fit extract yields and char viscosity.

The coordination number in CPD is from NMR data. The NMR data indicate an average of 2.5–3 bridges and 1.5–2 side chains per aromatic cluster or a coordination number between 4 and 5. However, some of the bridges indicated by the NMR analysis may actually be loops or substituted rings (such as aniline). Such a high coordination number does not permit accurate prediction of pyridine extracts, meaning either that the NMR data include a significant number of loops or that the interpretation of pyridine extracts as coming from the lattice is erroneous. Alternatively, it is possible that in coal the initial distribution of bridges and side chains is not random, as described by the Bethe lattice. The formation of coal may favor clusters that have two bridges and two side chains. If this is the case, the appropriate coordination number for network decomposition is the number of possible bridges, not the sum of bridges and side chains.

The FG-DVC model specifies yields of all light gas species, with yields determined from thermogravimetric Fourier transform infrared (TG-FTIR) experiments [21,27]. This model also correlates cross-linking reactions with evolution of certain light gases [10,15]. Other models describe light gas evolution as part of the network by specifying the number of side chains per cluster in addition to the number of connecting bridges per cluster. This latter approach has been used successfully to determine total light gas yields as a function of coal type [12,14,16–19], but it has not been used to calculate individual species.

Devolatilization

The most dramatic effect of coal pyrolysis on coal combustion is the rapid release of volatile matter. Since many coals may release more than 50% of their mass as volatile matter, gas-phase volatile combustion significantly increases temperatures in a relatively short time. In certain burner geometries for pulverized coal, the mass released during devolatilization creates a local volume expansion that is large enough to influence near-burner fluid dynamics. The volatile yield also affects the amount of char that must be burned heterogeneously.

The total volatile yield is a function of coal type, temperature, heating rate, pressure, and particle size. Particle size effects become small at diameters below 200 μm and are usually ignored in pulverized coal applications. Particles larger than 1 mm, such as those used in fluidized bed applications, exhibit significant internal mass transfer limitations that can lead to tar secondary reactions and deposition inside the particle [28].

Although early data indicated no significant effect of heating rate on total volatile yield [29], recent experiments show a small increase in yield with increasing heating rate [30]. Heating rate effects can be explained by the competition between tar formation

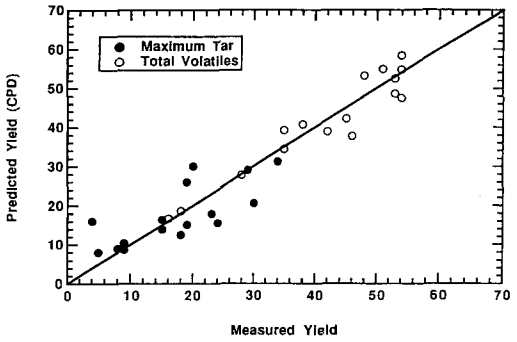

FIG. 2. Comparison of predicted and measured tar and total volatile yields using the CPD model with coal-dependent input coefficients directly from solid-state ^{13}C NMR data for 16 coals for a range of heating rates (0.5–10^4 K/s) and temperatures (1000–1300 K) [19].

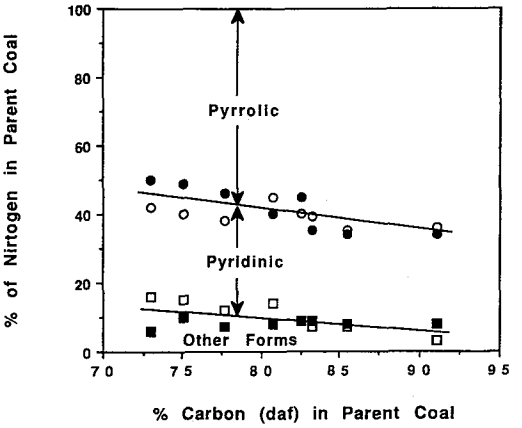

FIG. 3. Comparison of forms of nitrogen in the Argonne Premium coals as analyzed by XPS [43] (open symbols) and by XANES [44] (solid symbols).

(bridge breaking), tar destruction (cross-linking), and tar evolution (mass transfer), all of which depend differently on temperature [10]. At high heating rates, depending on particle size, internal heat transfer limitations become important, and particles may exhibit large internal temperature gradients [31].

The rate of devolatilization is sometimes thought to have little impact on comprehensive pulverized coal combustion models, since it happens so rapidly. However, it has been shown that using an unrealistic rate can affect the prediction of the flame zone near the burner, particularly in swirling flows [32,33]. Determination of devolatilization rates is hampered by the fact that mass release occurs during particle heat-up, and reported rates at a given heating rate vary by three orders of magnitude [34]. The large range in reported rates is due to the lack of temperature measurements during devolatilization [34,35]. Measurements of particle temperature during devolatilization, using FTIR emission/transmission particle cloud measurements [36] and single-particle two-color infrared pyrometry measurements [37,38], have substantially reduced the uncertainty in rates.

The network models have been successful in relating chemical features of parent coals to the pyrolysis behavior. For example, ^{13}C NMR measurements of four key chemical features of 16 coals were used directly (i.e., no adjustable coal-dependent parameters) in the CPD model to predict tar and total volatile yields for a wide range of pyrolysis temperatures and heating rates [19], as shown in Fig. 2. Methods have been developed for both the FLASHCHAIN and FG-DVC models for predicting input coefficients from elemental composition. These show reasonable success in predicting tar and total volatile yields [39–41]. A more detailed scheme is required to deduce input coefficients for models that predict light gas species as well as tar yields [21,40]. Network models of coal pyrolysis have successfully been used to calculate coal-dependent rates and yields of light gas and tar as a function of temperature, heating rate, and pressure.

Nitrogen Release

The amount of nitrogen released from the coal during devolatilization, along with the form of the nitrogen species and transformation to NO_x precursors such as HCN and NH_3, is important to pollutant control strategies. For example, low-NO_x burners work on the principle that the devolatilized nitrogen species will form N_2 rather than NO_x under locally fuel-rich conditions. The form of nitrogen in the coal, particularly if it is entirely contained in aromatic groups or in peripheral side chains, determines the nitrogen species released during devolatilization. Coal nitrogen is thought to occur mainly in five-member (pyrrolic) or six-member (pyridinic) aromatic ring structures [42–44]. Both x-ray photoelectron spectroscopy (XPS) and x-ray absorption near-edge structure (XANES) spectroscopy indicate the presence of additional species that may include quaternary nitrogen or aromatic amines. Figure 3 shows the quantitative agreement between XPS and XANES analyses of the major forms of nitrogen in the Argonne Premium coals. Pyrrolic nitrogen is the most common form, followed by pyridinic for all coal ranks; other forms are relatively small. Davidson [45] provides a more detailed review of the forms of nitrogen in coal.

Nitrogen release during devolatilization is a function of final temperature [46,47], even though the total devolatilization yield may increase only slightly after a certain temperature, as shown in Fig. 4. The high-temperature nitrogen release is due to graphitization-type reactions, where the char becomes

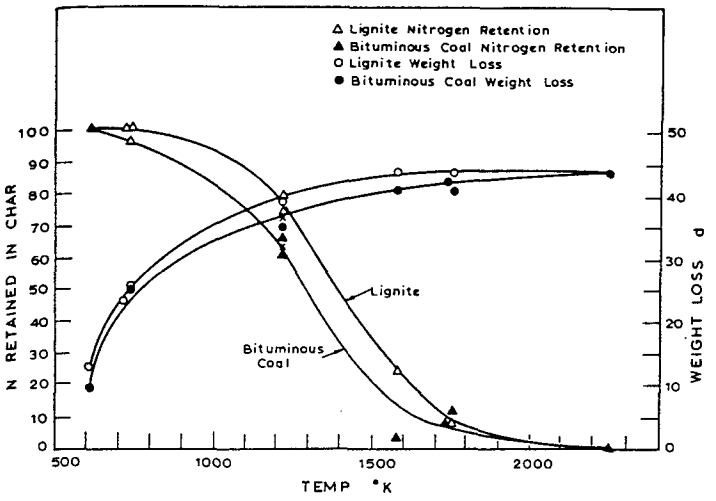

FIG. 4. Nitrogen retention in char and weight loss (dry) for coal heated in crucibles as a function of temperature [45].

more aromatic and releases heteroatoms preferentially to carbon. Nitrogen release increases with increasing heating rate and decreases with increasing pressure [48].

Two questions arise regarding nitrogen release: (a) what are the primary devolatilization products and (b) what are the products after secondary pyrolysis. Of interest is the amount of HCN and NH_3 formed, since detailed models exist to describe the reaction chemistry of HCN and NH_3 to form NO_x [49]. Since nitrogen in the parent coal exists mainly in aromatic ring structures, it is logical to assume that the nitrogen release occurs mainly in tar molecules during tar release and then as light gases during high-temperature graphitization reactions [50,51].

At rapid heating rates (>1000 K/s) and temperatures lower than 700 °C, HCN is not a primary product [50–53]. Even at rapid heating rates, tar release generally occurs before any HCN is released. No NH_3 is generally seen during rapid pyrolysis in heated grid experiments [51] or entrained flow experiments [52,53]. However, Kambara et al. [54] recently measured NH_3 yields during devolatilization at 1000 K/s and correlated these yields with quaternary nitrogen content. Nelson et al. [42] also reported NH_3 yields from devolatilization in a fluidized bed reactor with estimated initial heating rates of 10^4 K/s.

At low heating rates, such as in thermogravimetric analysis (TGA) devolatilization experiments at 30 °C/s, both HCN and NH_3 are measured, with a dominance of NH_3 rather than HCN [53]. Low rank coals release a larger fraction of nitrogen as HCN and NH_3 than high rank coals at these low heating rates. Bassilakis and coworkers [53] rationalize that the NH_3 evolution observed at low heating rates is due to the conversion of HCN to NH_3 in the pores of the char, with hydrogen donation from the solid char. A model was developed to describe the conversion of HCN to NH_3 inside the coal particle, based on the residence time of light gas inside the particle [53]. This model was used to explain the NH_3 yields observed in TGA experiments and in Nelson's fluidized bed coal pyrolysis experiments [42]. In Nelson's lower-temperature experiments, the NH_3 is formed when the coal particle is at or near the bed temperature and the heating rate has slowed down considerably.

Secondary pyrolysis of coal tar and light gases results in the formation of HCN and soot. Chen and Niksa [52] showed that the soot can initially contain a significant amount of nitrogen, since it is formed from vaporized tar that often contains most of the devolatilized nitrogen. At increased temperatures, the fraction of nitrogen contained in the soot decreases as heteroatoms are expelled due to graphitization reactions. Secondary pyrolysis of tar and soot are, therefore, important to understanding nitrogen species evolution during volatile combustion.

The amount of nitrogen evolved at a given temperature and heating rate is a function of coal rank but is not proportional to the tar yield. Figure 5 shows total nitrogen release as a function of carbon content of the parent coal in flat flame methane burner experiments [55]. Heating rates in this experiment were approximately 5×10^4 K/s, and particle temperatures reached approximately 1400 K. Tar yields from lignites (<70% carbon) are significantly lower than from high volatile bituminous coals (75–80% carbon), yet the two coals release comparable fractions of nitrogen during pyrolysis. This is consistent with the observations that low rank coals (which have low tar yields) release a larger fraction of nitrogen as light gas than do medium rank coals (which have high tar yields). Only the low volatile bituminous coals (85–90% carbon) exhibit low amounts of nitrogen release.

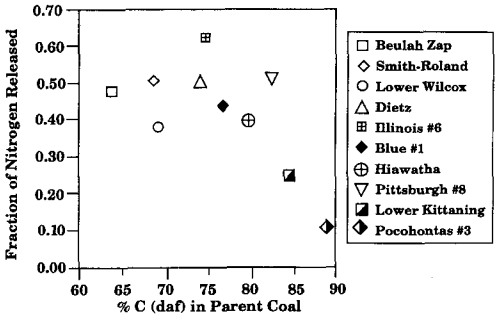

FIG. 5. Fraction of nitrogen released during devolatilization as a function of coal rank (i.e., carbon content) in flat flame methane burner experiments in 6 mole% post-flame oxygen [55]. Residence times were 47 ms, and the heating rate was approximately 5×10^4 K/s. Samples were taken prior to significant char oxidation.

Softening and Swelling

The swelling of coal is important in combustion because it affects the char particle's size and porosity and, hence, its trajectory, ignition, reactivity, fragmentation, and ash size distribution. Swelling occurs during pyrolysis in coals, which soften, and is caused by the evolution of gases, which form bubbles that expand within the softened particles. For fluidized or fixed beds, in which large coal particles heat relatively slowly, particle diameters can increase. For PC firing, particle sizes may not increase due to the high heating rates, but significant changes occur in the char morphology due to bubble formation. The most complete description of bubble formation is the multi-bubble model of Oh et al. [56], which includes the effect of bubble growth, bubble transport to the surface, and diffusion of gases through the liquid. The following discussion considers softening first and then bubble formation.

Softening:

The softening of coal is most often measured at low heating rates with a Giessler Plastometer [57]. Data at higher temperatures have been obtained by Fong et al. [58] in a device designed for rapid heating. Both the slow and fast heating rate results exhibit an increase in fluidity as the coal melts and pyrolyzes, followed by a decrease as the char solidifies (see Fig. 6c). As demonstrated by Fong et al. [58] and Oh et al. [56], the maximum in fluidity is associated with a maximum in extractable molecules. Proton magnetic resonance thermal analysis (PMRTA) experiments of Lynch et al. [59,60], which measure the fraction of mobile molecules in the coal, show a corresponding maximum in the "mobile fraction" in the coal (Fig. 6a). In the language of the network models, the increase in fluidity is associated with the thermal decomposition of the network, while the subsequent decrease is associated with the network recondensation or cross-linking.

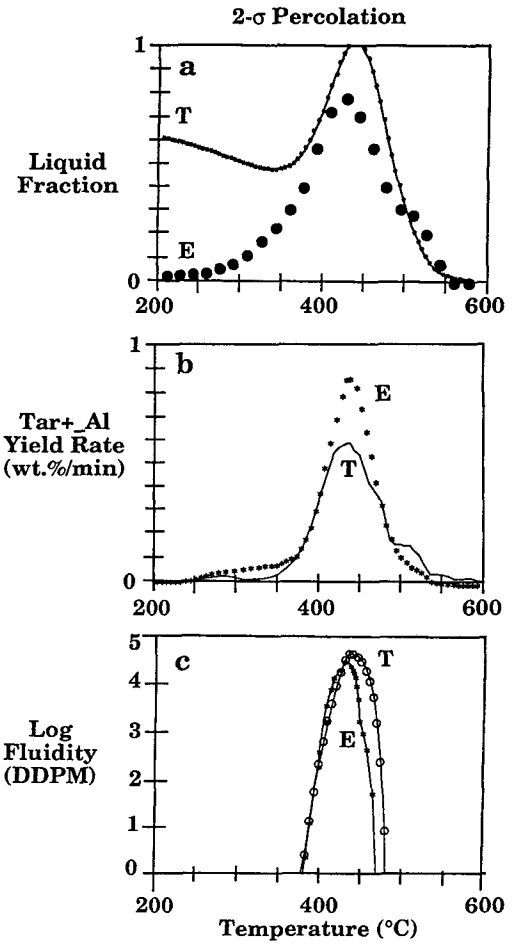

FIG. 6. Comparison of 2-σ percolation theory for liquid fraction, tar yield rate, and Gieseler fluidity for Pittsburgh No. 8 bituminous coal pyrolyzed at 3 K/min^{-1}. T = theory; E = experimental data [21].

There are a number of factors that contribute to the softening of coal. van Krevelen and coworkers [61,62] and Neavel [63] relate the fluidity of coal to the detached molecular fraction called "metaplast." The factors that control the particle's fluidity include (1) the fraction of metaplast formed; (2) the fluidity of the metaplast fraction; (3) the dependence of this fluidity on temperature; (4) the contributions of suspended solids in the metaplast, both "chunks" of char and mineral particles; and (5) the formation of bubbles due to trapped gases.

Several models for coal viscosity have been proposed, which consider all of the influences except the bubbles. The models were based on the two-step

process described by Van Krevelen and coworkers [61,62], which assumes the following reactions to occur on heating:

$$\text{coal} \xrightarrow{k_1} \text{metaplast} \xrightarrow{k_2} \text{coke}.$$

Models for fluidity in which the rate of formation and destruction of metaplast is described by global rates k_1 and k_2 employ empirical expressions for viscosity as a function of the metaplast fraction [53,58,64].

Solomon et al. [20] also employ an empirical model for viscosity based on the metaplast fraction, but a network model [10,21] is used to predict the metaplast fraction. The metaplast is defined as the fraction of molecules that are not attached to the network. The increase in metaplast is associated with bond-breaking reactions, while the solidification is due to cross-linking. Low rank coals generally do not exhibit fluidity because the cross-linking reactions occur at lower temperatures than the bond-breaking reactions [15,65].

A comparison of theory and experiment for Giessler fluidity, tar yield, and the PMRTA liquid fraction is presented in Fig. 6 from Ref. 21. The data are compared to the FG-DVC 2-σ percolation model. For a single coal, these network models allow all of these events to be predicted at arbitrary heating rate and pressure with a single pair of kinetic rates for bond breaking and cross-linking. In Fig. 6a, the lack of agreement at low temperature is due to the fact that the model does not include the effect of temperature on the molecule's mobility.

The use of network models also makes it possible to understand why weathering (oxidation) is so effective in reducing fluidity [21]. The apparent reason is that oxidation leads to low-temperature cross-linking. Such cross-linking in a two-dimensional network increases the coordination number and is thus extremely effective in reducing metaplast fraction.

Swelling:

Swelling models have been developed by several investigators [56,66–68]. The basic physics is contained in the single bubble model of Chiou and Levine [66], who considered the swelling rate of a pulverized coal particle of external radius r_2 with a single void of radius r_1 with spherical symmetry. The swelling they depict is due to the pressure of trapped evolved gases, doing work against viscous forces. The pressure within a bubble can be determined from the rate of gas evolution predicted by a pyrolysis model and an assumed diffusion rate of gases through the liquid. In the work of Zhao and Best [68], the viscosity was predicted as in Ref. 20. Two additional parameters were also required to describe the effect of bubble bursting that limits swelling at high heating rates: a critical bubble wall stress and the wall surface tension.

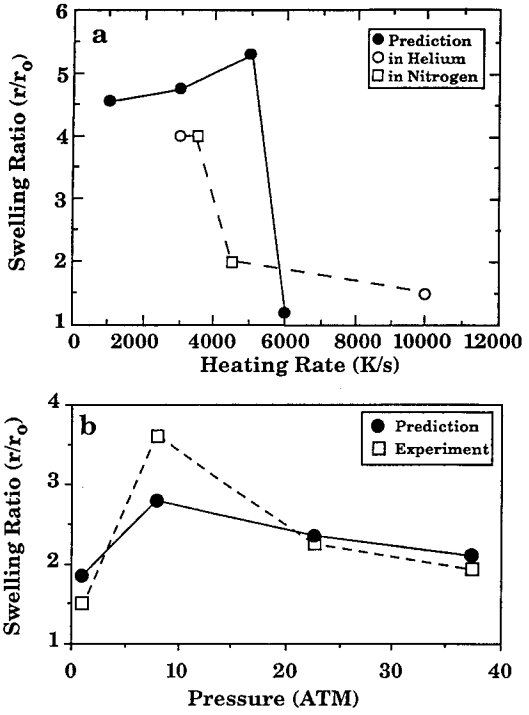

FIG. 7. (a) Comparison of experimental data (open symbols) and predicted (closed symbols) particle swelling ratios as a function of heating rate and (b) comparison of model prediction (closed symbols) and experiment (open symbols) [71] for swelling ratio vs ambiant pressure, for Illinois No. 6 coal (nominal rad = 31 μm), at a heating rate between 1000 and 1150 K/s.

According to the above model [68], a bubble grows until the rate of gas filling the bubble equals the rate of diffusion through the wall or else until the pressure difference across the wall exceeds the critical wall stress and the bubble ruptures. Experimental observations for the swelling ratio (r/r_0) of final radius r to initial radius r_0 and predictions are presented in Fig. 7a. For a heating rate of 5000 °C/s and below, cenospheres are formed, and the swelling ratio can be as high as 4. The model of Oh et al. [56] predicts a similar swelling ratio. At heating rates above 5000 °C/s, the evolution of gas is too fast and the bubbles rupture, reducing the swelling. This rupture phenomenon, which has been observed experimentally [67,69,70], is not included in Oh's model [56].

Figure 7b compares the theory and experiment [71] for the swelling ratio of an Illinois no. 6 coal as a function of pressure. With increasing pressure, the more volatile components of tar are held in the particles for longer times, decreasing viscosity at the critical time of gas evolution and increasing (r/r_0). With a further increase in pressure, the compressive external envi-

ronment results in a reduction in swelling. Similar results at high pressure were predicted by Oh et al. [56].

Secondary Pyrolysis and Soot Formation

Secondary pyrolysis of coal devolatilization products in fuel-rich regions of coal flames produce significant amounts of soot. The soot in the flame region thermally radiates heat to cooler regions of the furnace and therefore cools the flame. Since furnace walls are generally cooler than the flame temperature, the presence of soot may cool the flame by several hundred degrees. Predictions of the flame temperatures resulting from volatile combustion must, therefore, account for soot radiation.

While soot from combustion of pure hydrocarbons has been studied extensively, relatively little is known about coal-derived soot. Coal tar contains aromatic compounds with average molecular weights in the range of 350 amu, and therefore, the mechanism for soot formation from coal tar differs from combustion of fuels such as butane and acetylene, which require the formation of aromatic rings. Contrails of soot were visualized in single-particle combustion experiments by McLean et al. [72] and by Seeker et al. [73]. A single-particle model, including a local soot cloud, was developed by Lau and Niksa [74]. A model for secondary reactions of coal tar was developed based on homogeneous cracking of tar produced in a packed bed reactor [75].

Pyrolysis-induced soot formation experiments have shown the beginnings of chemical structure changes leading to soot formation [76–79]. Wornat and coworkers [78] defined soot yield as the devolatilization products that were not soluble in dichloromethane. Their results for a Pittsburgh no. 8 coal indicated that soot yields increased with both residence time and temperature, while the soluble fraction of the coal tars decreased proportionally. Related experiments by Chen et al., [79], using tetrahydrofuran (THF) as the solvent, showed similar results for a Pittsburgh no. 8 coal and a Dietz subbituminous coal. Both Wornat's and Chen's data indicate that while soot yields increase with temperature, the total yield of soot plus tar remains constant, as shown in Fig. 8.

Important radiative properties for modeling soot radiation are the soot volume fraction and the soot particle size. A thermophoretic sampling probe was used to sample soot and tar samples from a high-temperature pyrolysis experiment as a function of residence time [80]. Preliminary results indicate that initial soot particles formed are approximately 25 nm in diameter, while agglomerates reach sizes of 200–800 nm in 130 ms. This is different behavior than observed in the single-particle combustion experiments [72,73], where the flame around individual particles causes soot particles to form in contrails. When the tar is free to expand in a cloud away from the particle, such as in a pyrolysis experiment or in a fuel-rich cloud, the soot does not form such contrails.

A study employed an FTIR to study soot concentrations in flames [81,82]. A comparison of the soot concentration (proportional to the attenuation of infrared radiation across the flame) for three samples is shown in Fig. 9a. The demineralized Rosebud (which has twice the tar yield of the raw Rosebud) produces about twice the maximum soot yield compared to the raw sample. The char (which has no tar) produces almost none. As shown in Fig. 9b, the soot production increases with the yield of tar as determined in pyrolysis experiments [81]. This relationship between tar and soot is consistent with other results [78,79,83].

Char Reactivity

This section is concerned with the effect of coal pyrolysis on char reactivity. Space limitations allow for only a brief qualitative discussion. There are two important effects: physical and chemical.

The physical effects determine the char morphology. The plastic properties of the coal affect the size of the char particle and its pore distribution. The pore distribution determines the diffusion of reactants within the particle, which is often a rate-limiting step for char oxidation.

The chemical effects of pyrolysis determine the char's intrinsic reactivity. The intrinsic reactivity controls the char burning rate in zone I (the kinetic region) and affects zone II (the pore diffusion region). Theoretically, the condensation of the coal's macromolecular network at the latter stages of pyrolysis leads to a reduction in the active site density, which reduces the intrinsic char reactivity. Experimentally, intrinsic reactivities are observed to decrease with the increasing extent of pyrolysis [85–88] and seem to correlate with the aromatic hydrogen concentration of the char [84]. In low rank coals (oxygen concentration greater than 13%), several studies [84,89,90] show that organically bound alkali and alkaline earth metals (especially calcium) control the intrinsic oxidation when measured at low temperature.

Conclusion

The pyrolysis process has impacts throughout coal combustion. The devolatilization yield affects the initial amount of char that must be oxidized. The rate of devolatilization can affect the near-burner structure of the flame. The nitrogen release during devolatilization is important to low-NO_x burner strategies. The pyrolysis product distribution, particularly the amount of tar, affects the amount of soot pro-

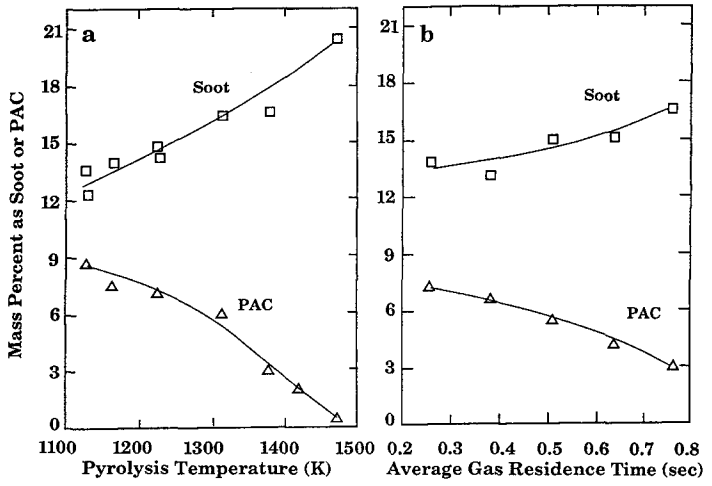

FIG. 8. Soot and soluble polyaromatic compound (PAC) yields under various pyrolysis conditions: (a) experiment set 1, residence time = 0.75 s; (b) experiment set 2, temperature = 1375 K [78].

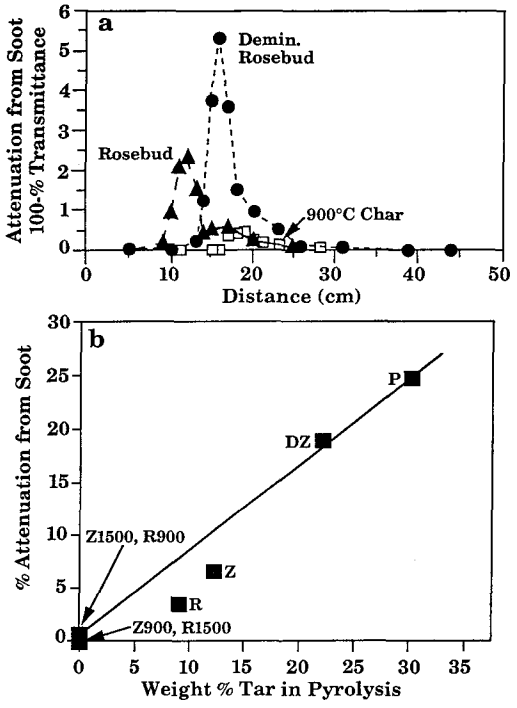

FIG. 9. Correlation of soot production with tar yield. (a) Comparison of soot attenuation for three samples burned in a flame stabilized by preheated air and (b) correlation of the maximum soot attenuation with tar yield in pyrolysis in an entrained flow reactor. P = Pittsburgh; DZ = demineralized zap; Z = zap; R = Rosebud; numbers are pyrolysis temperature for char [81].

duced, which in turn affects the temperature in the flame zone due to radiative loss. The softening behavior of the coal during pyrolysis affects the size, porosity, and internal surface area of the char, which affect the high-temperature reactivity. Detailed pyrolysis models have been developed based on the chemical structure of coal. The network pyrolysis models have shown the ability to quantitatively predict many of these major pyrolysis phenomena.

Acknowledgments

Work done at Advanced Fuel Research, Inc. was sponsored under Contract No. DE-AC21-86MC23075 with the U.S. Department of Energy Morgantown Energy Technology Center. The work at Brigham Young University was sponsored in part by the Advanced Combustion Engineering Research Center, funded by the National Science Foundation, the State of Utah, 31 industrial participants, and the U.S. Department of Energy. The authors would like to thank Dr. M. A. Serio, Dr. Y. Zhao, Ms. S. Charpenay, and Mr. M. L. Tanner for their help on the manuscript.

REFERENCES

1. Gavalas, G. R., *Coal Pyrolysis*, Elsevier, Amsterdam, 1982, p. 51.
2. Gavalas, G. R., Cheong, P. H., and Jain, R., *Ind. Eng. Chem. Fundam.* 20:122 (1981).
3. Solomon, P. R., and King, H. H., *Fuel* 63:1302 (1984).
4. Solomon, P. R., Squire, K. R., and Carangelo, R. M., *Proceedings of the International Conference on Coal Sciences*, Peragom, Sydney, Australia, 1985, p. 945.

5. Squire, K. R., Carangelo, R. M., DiTaranto, M. B., and Solomon, P. R., *Fuel* 65:833 (1986).
6. Niksa, S., and Kerstein, A. R., *Combust. Flame* 66:95 (1986).
7. Niksa, S., *Combust. Flame* 66:111 (1986).
8. Niksa, S., and Kerstein, A. R., *Fuel* 66:1389 (1987).
9. Niksa, S., Kerstein, A. R., and Fletcher, T. H., *Combust. Flame* 69:221–228 (1987).
10. Solomon, P. R., Hamblen, D. G., Carangelo, R. M., Serio, M. A., and Deshpande, G. V., *Energy Fuels* 2:405 (1988).
11. Niksa, S., *AIChE J.* 34:790 (1988).
12. Grant, D. M., Pugmire, R. J., Fletcher, T. H., and Kerstein, A. R., *Energy Fuels* 3:175 (1989).
13. Solomon, P. R., Hamblen, D. G., Yu, Z. Z., and Serio, M. A., *Fuel* 69:754 (1990).
14. Fletcher, T. H., Kerstein, A. R., Pugmire, R. J., and Grant, D. M., *Energy Fuels* 4:54 (1990).
15. Solomon, P. R., Serio, M. A., Desphande, G. V., and Kroo, E., *Energy Fuels* 4:42 (1990).
16. Niksa, S., and Kerstein, A. R., *Energy Fuels* 6:647–665 (1991).
17. Niksa, S., *Energy Fuels* 5:665–673 (1991).
18. Niksa, S., *Energy Fuels* 5:673–683 (1991).
19. Fletcher, T. H., Kerstein, A. R., Pugmire, R. J., Solum, M. S., and Grant, D. M., *Energy Fuels* 6:414–431 (1992).
20. Solomon, P. R., Best, P. E., Yu, Z. Z., and Charpenay, S., *Energy Fuels* 6:143–154 (1992).
21. Solomon, P. R., Hamblen, D. G., Serio, M. A., Yu, Z. Z., and Charpenay, S., *Fuel* 72 (4):469–488 (1993).
22. Smith, K. L., Smoot, L. D., Fletcher, T. H., and Pugmire, R. J., *The Structure and Reaction Processes of Coal,* Plenum, New York, 1994, pp. 273–323.
23. Suuberg, E. M., Unger, P. E., and Lilly, W. D., *Fuel* 64:956 (1985).
24. Fletcher, T. H., Grant, D. M., and Pugmire, R. J., *ACS Div. Fuel Chem. Preprints* 36 (1):250–257 (1991).
25. Solum, M. S., Pugmire, R. J., and Grant, D. M., *Energy Fuels* 3:187 (1989).
26. Orendt, A. M., Solum, M. S., Sethi, N. K., Pugmire, R. J., and Grant, D. M., *Advances in Coal Spectroscopy* (H. L. C. Meuzelaar, Ed.), Plenum Press, New York, 1992, pp. 215–254.
27. Solomon, P. R., Serio, M. A., Carangelo, R. M., Bassilakis, R., Gravel, D., Baillargeon, M., Baudais, F., and Vail, G., *Energy Fuels* 4:319–333 (1990).
28. Saxena, S. C., *PECS* 16:55–94 (1990).
29. Anthony, D. B., Howard, J. B., Hottel, H. C., and Meissner, H. P., *Fifteenth Symposium (International) on Combustion,* The Combustion Institute, Pittsburgh, 1974, pp. 1303–1317.
30. Gibbins-Matham, J., and Kandiyoti, R., *Energy Fuels* 2:505–511 (1988).
31. Hertzberg, M., Zlochower, I. A., and Edwards, J. C., "Coal Particle Pyrolysis Mechanisms and Temperatures," Bureau of Mines Report 9169, 1988.
32. Smith, J. D., Smith, P. J., and Hill, S. C., *AIChE J.* 39:1668–1679 (1993).
33. Fletcher, T. H., "Sensitivity of Combustion Calculations to Devolatilization Rate Expressions" presented at the AFRC Fall Meeting, Sandia National Laboratories, Livermore, CA, Sandia Report No. SAND85-8854, available NTIS, 1985.
34. Solomon, P. R., Fletcher, T. H., and Pugmire, R. J., *Fuel* 72:587–597 (1993).
35. Freihaut, J. D., and Proscia, W. M., *Energy Fuels* 3:625 (1989).
36. Solomon, P. R., Serio, M. A., Carangelo, R. M., and Markham, J. R., *Fuel* 65:182–194 (1986).
37. Fletcher, T. H., *Combust. Sci. Technol.* 63:89–105 (1989).
38. Fletcher, T. H., *Combust. Flame* 78:223–236 (1989).
39. Niksa, S., and Kerstein, A. R., *Proceedings of the International Conference on Coal Science,* Banff, Canada, 1993, Vol. 2, pp. 397–400.
40. Zhao, Y., Serio, M. A., and Solomon, P. R., *ACS Div. Fuel Chem. Preprints* 39:(1994); see also Zhao, Y., Serio, M. A., and Solomon, P. R., "A Method of Predicting Coal Devolatilization Behavior Based on Coal Elemental Compositions," submitted to the *Twenty-Fifth Symposium (International) on Combustion,* The Combustion Institute, Pittsburgh, (1994).
41. Niksa S., *Energy Fuels* 8:659–670 (1994); see also Niksa, S., "Predicting the Devolatilization Behavior of any Coal from its Ultimate Analysis," *Twenty-Fifth Symposium (International) on Combustion,* The Combustion Institute, Pittsburgh, 1994.
42. Nelson, P. F., Buckley, A. N., and Kelly, M. D., *Twenty-Fourth Symposium (International) on Combustion,* The Combustion Institute, Pittsburgh, 1992, pp. 1259–1267.
43. Kelemen, S. R., Gorbaty, M. L., Vaughn, S. N., and Kwiatek, P. J., *ACS Div. Fuel Chem. Preprints* 38 (2):384–392 (1993).
44. Mitra-Kirtley, S., Mullins, O. C., Branthaver, J., van Elp, J., and Cramer, S. P., *ACS Div. Fuel Chem. Preprints* 39 (2):762–768 (1993).
45. Davidson, R. U., "Nitrogen in Coal," IEA Report No. IEAPER/08 1994.
46. Pohl, J. H., and Sarofim, A. F., *Sixteenth Symposium (International) on Combustion,* The Combustion Institute, Pittsburgh, 1976, pp. 491–501.
47. Blair, D. W., Wendt, J. O. L., and Bartok, W., *Sixteenth Symposium (International) on Combustion,* The Combustion Institute, Pittsburgh, 1976, pp. 475–489.
48. Cai, H. Y., Guell, A. J., Dugwell, D. R., and Kandiyoti, R., *Fuel* 72:321–327 (1993).
49. Miller, J. A., and Bowman, C. T., *PECS* 15:287–338 (1989).
50. Solomon, P. R., and Colket, M. B., *Fuel* 57:749–755 (1978).
51. Freihaut, J. D., Proscia, W. M., and Mackie, J. C., *Combust. Sci. Technol.* 93:323–347 (1993).
52. Chen, J. C., and Niksa, S., *Energy Fuels* 6:254–264 (1992).
53. Bassilakis, R., Zhao, Y., Solomon, P. R., and Serio, M. A., *Energy Fuels* 7:710–720 (1993).

54. Kambara, S., Takarada, T., Yamamoto, Y., and Kato, K., *Energy Fuels* 7:1013–1020 (1993).
55. Mitchell, R. E., Hurt, R. H., Baxter, L. L., and Hardesty, D. R., "Compilation of Sandia Coal Char Combustion Data and Kinetic Analysis," Sandia Report SAND92-8208, available NTIS (1992).
56. Oh, M. S., Peters, W. A., and Howard, J. B., *AIChE J.* 35:5 775–792 (1989).
57. ASTM D 2639-74 (reapproved 1980).
58. Fong, W. S., Khalil, Y. F., Peters, W. A., and Howard, J. B., *Fuel* 65:195 (1986).
59. Lynch, L. J., Sakurovs, R., Webster, D. S., and Redlich, P. J., *Fuel* 67:1036 (1988).
60. Lynch, L. J., Webster, D. S., Sakurovs, R., Barton, W. A., and Maher, T. P., *Fuel* 67:579 (1988).
61. van Krevelen, D. W., *Coal*, Elsevier, Amsterdam, 1961.
62. Chermin, H. A. G., and van Krevelen, D. W., *Fuel* 36:85 (1957).
63. Neavel, R. C., in "Coal Plasticity Mechanism: Inferences from Liquefaction Studies" (M. L. Gorbaty, J. W. Larsen, and I. Wender, Eds.), *Coal Science 1*, Academic Press, New York, 1982.
64. Franked, N. A., and Acrivos, A., *Chem. Eng. Sci.* 22:847 (1976).
65. Suuberg, E. M., Lee, D., and Larsen, J. W., *Fuel* 64:1668 (1985).
66. Chiou, M. J., and Levine, H. B., "Investigation of Structure Deformation of Coal Particles in Pyrolysis" Report from Jaycor.
67. Solomon, P. R., and Hamblen, D. G., *Chemistry of Coal Conversion* (R. H. Schlosberg, Ed.), Plenum Publishing, New York, 1985, pp. 121–151.
68. Zhao, Y., and Best, P. E., "Measurement and Modeling of Advanced Coal Conversion Processes," Final Report, U.S. DoE/METC Contract No. DE-AC21-86MC23075, 1993.
69. Pohl, J. M., Kobayashi, H., and Sarofim, A. F., "The Effects of Temperature and Time on the Swelling of Pulverized Coal Particles", Industrial Liason Program, Symposium Paper, MIT, Oct. 2, 1979.
70. Gale, T. K., Bartholomew, C. H., and Fletcher, T. H., "Decreases in the Swelling and Porosity of Bituminous Coals During Devolatilization at High Heating Rates," *Combust. Flame* (1994), accepted.
71. Lee, C. W., Scaroni, A. W., and Jenkins, R. G., *Fuel* 70:957 (1991).
72. McLean, W. J., Hardesty, D. R., and Pohl, J. H., *Eighteenth Symposium (International) on Combustion*, The Combustion Institute, Pittsburgh, 1980, p. 1239.
73. Seeker, W. R., Samuelson, G. S., Heap, M. P., and Trolinger, J. D., *Eighteenth Symposium (International) on Combustion*, The Combustion Institute, Pittsburgh, 1980, p. 1213.
74. Lau, C. W., and Niksa, S., *Combust. Flame* 95:1–21 (1993).
75. Serio, M. A., Peters, W. A., and Howard, J. B., *Industr. Eng. Chem. Res.* 26:1831–1838 (1987).
76. Fletcher, T. H., Solum, M. S., Grant, D. M., Critchfield, S., and Pugmire, R. J., *Twenty-Third Symposium (International) on Combustion*, The Combustion Institute, Pittsburgh, 1990, p. 123.
77. Pugmire, R. J., Solum, M. S., Grant, D. M., Critchfield, S., and Fletcher, T. H., *Fuel* 70:414–423 (1991).
78. Wornat, M. J., Sarofim, A. F., and Longwell, J. P., *Energy Fuels* 1:431 (1987).
79. Chen, J. C., Castagnoli, C., and Niksa, S., *Energy Fuels* 6:264–271 (1992).
80. Ma, J., Dean, M., Rossman, J., Sastrawinata, T., Webb, B., and Fletcher, T. H., "Properties of Soot from Coal," presented at the Fall 1993 WSS/CI Meeting, SRI, Menlo Park, CA, Oct. 18–19, 1993.
81. Solomon, P. R., Chien, P. L., Carangelo, R. M., Best, P. E., and Markham, J. R., *Twenty-Second Symposium (International) on Combustion*, The Combustion Institute, Pittsburgh, 1988, pp. 211–221.
82. Brewster, B. S., Smoot, L. D., Solomon, P. R., and Markham, J. R., *Energy Fuels* 7:884–890 (1993).
83. Nenniger, R. D., Howard, J. B., and Sarofim, A. F., *Proceedings of the 1983 International Conference on Coal Science*, Pittsburgh, PA, Aug. 15–19, 1983, p. 521.
84. Charpenay, S., Serio, M. A., and Solomon, P. R., *Twenty-Fourth Symposium (International) on Combustion*, The Combustion Institute, Pittsburgh, 1992, pp. 1189–1197.
85. Best, P. E., Solomon, P. R., Serio, M. A., Suuberg, E. M., Mott, W. R., Jr., and Bassilakis, R., *ACS Div. Fuel Chem. Preprints* 32 (4):138 (1987).
86. Khan, R., *Fuel* 66:1626 (1987).
87. Radovic, L. R., Walker, P. L., and Jenkins, R. G., *Fuel* 62:1209 (1983).
88. Radovic, L. R., Walker, P. L., and Jenkins, R. G., *Fuel* 62:849 (1983).
89. Floess, J. K., Longwell, J. P., and Sarofim, A. F., *Energy Fuels* 2:756–764 (1988).
90. Solomon, P. R., Serio, M. A., and Henninger, S. G., *ACS Div. Fuel Chem. Preprints* 31 (3):200 (1986).

COMMENTS

Stephen Niksa, SRI International, USA. I appreciate your even-handed coverage of the futures that our models have in common. However, nominal rates of devolatilization based on a single first-order chemical reaction that you report for your BYU and AFR data have magnitudes and activation energies that are much higher than those that have been reported during the past three decades. Now that FLASHCHAIN predictions explain the lower rates without resorting to heat or mass transport resistances [1], there is an enormous body of experimental and modeling

results that contradict your values. Your values do not reconcile any discrepancies because there is so much information that disagrees with them.

REFERENCE

1. Niksa, S., *Energy Fuels* 8:670 (1994).

Author's Reply. During the past three decades, most kinetic rates reported in the literature for coal pyrolysis reactions have been measured in experiments where the coal particle temperatures were estimated, not measured. In most cases, rates were reported only for a narrow range of heating rates. This resulted in wide discrepancies in reported rates and activation energies even for similar coals under nominally the same heating rates and temperatures. Investigation of the discrepancies leads to the conclusion that particle temperatures were inaccurately estimated in many cases [1–3]. When particle temperatures were measured, the rates are at the high end of the range that is in the literature [4–7]. When a distributed activation energy model (DAEM) is used to fit data over a range of heating rates, the frequency factors are in the range of 10^{13}–10^{15} s^{-1} and the activation energies are in the range of 45–60 kcal. DAEM models of this kind do fit data over a wide range of heating rates.

Niksa's FLASHCHAIN predictions [8] do not explain the lower rates, they simply show that a chemical reaction with a distribution of rates will yield a low apparent activation energy when fit with a single rate model over a narrow range of heating rates. This fact is well known and has been discussed in many previous publications by others. We agree with Niksa that there is a large body of results that contradict the values that were presented in our presentation, but none of the contradicting results were obtained with coal particle measurements.

REFERENCES

1. Freihaut, J. D., and Proscia, W. M., *Energy Fuels* 3:625 (1989).
2. Solomon, P. R., Serio, M. A., and Suuberg, E. M., *Prog. Energy Combust. Sci.* 18:133–220 (1992).
3. Solomon, P. R., Fletcher, T. H., and Pugmire, R. J., *Fuel* 72:587–597 (1993).
4. Solomon, P. R., Serio, M. A., Carangelo, R. M., and Markham, J. R., *Fuel* 65:182 (1986).
5. Serio, M. A., Hamblen, D. G., Markham, J. R., and Solomon, P. R., *Energy Fuels* 1:138 (1987).
6. Fletcher, T. H., *Combust. Sci. Technol.* 63:89–105 (1989).
7. Fletcher, T. H., *Combust. Flame* 78:223–236 (1989).
8. Niksa, S., *Energy Fuels* 8:670 (1994).

•

Larry Baxter, Sandia National Laboratories, USA. Are there relationships between the parameters used in the network devolatilization models (C^{13} nmr, FTIR, extra four yields, etc.) and traditional descriptions of coal in terms of maceral groups?

Author's Reply. The relationships between the parameters used in network devolatilization models and measurements of the heterogeneity of coal, such as maceral groups and microlithotypes, have not been explored in great detail. Maceral concentrates have, however, been analyzed by ^{13}C NMR, FTIR, and other techniques. For example, carbon aromaticity in maceral groups follows in the order: inertinite > vitrinite > exinite. Parameters used in current network models represent only average properties of the coal.